

# Topological phases of the Bogoliubov de Gennes Hamiltonian

Klaus Ziegler<sup>1,2</sup>

<sup>1</sup>Institut für Physik, Universität Augsburg  
D-86135 Augsburg, Germany

<sup>2</sup>Physics Department, New York City College of Technology  
The City University of New York  
Brooklyn, NY 11201, USA

(Dated: March 13, 2026)

We investigate a two-dimensional superconducting system with a smoothly and periodically varying order parameter. The order parameter is modulated along one direction while remaining uniform in the perpendicular direction, leading to a spatially periodic superconducting phase. We show that the periodicity of the order parameter determines the winding number of the eigenfunctions, which serves as a topological characterization of the system. A topological invariant is identified that links the winding number directly with the Bloch vector. By solving the Bogoliubov–de Gennes equation, we obtain both plane-wave solutions describing bulk states and exponentially localized solutions that correspond to edge modes. The analytic bulk–edge connection is employed to identify the conditions under which the edge states emerge from the bulk spectrum. We find that the winding numbers depend on the boundary conditions, which differ between the plane-wave and exponential solutions. These results establish a direct connection between the spatial modulation of the order parameter, the topological structure of the eigenstates, and the emergence of edge modes in periodically modulated superconducting order parameters.

## I. INTRODUCTION

Quasiparticles in a superconductor are described by the Bogoliubov de Gennes (BdG) Hamiltonian, which represents a two-band model. There is a gap  $2|\Delta|$  between these bands, which is determined by the density of the superconducting electrons through the magnitude of the superconducting order parameter  $|\Delta|$ . The order parameter itself has a phase factor, such that  $\Delta = |\Delta|e^{i\varphi}$  describes the superconducting state. The model of the superconductor is invariant under a global phase shift  $\varphi \rightarrow \varphi + \varphi_0$ . Thus, we can remove a uniform phase by such a shift operation, which means that a uniform phase is not observable. A spatially non-uniform phase, on the other hand, cannot be removed by a global phase shift. It turns out that it is observable and related to a gauge field in which the electrons move. A typical example is an external magnetic field (e.g., the Abrikosov lattice of a type II superconductor [1]). Other examples for a system with a spatially varying order-parameter phase are Josephson junctions [2–4]. For the following, we are mostly interested in a periodically changing order-parameter phase, as it appears in the Fulde-Ferrell-Larkin-Ovchinnikov (FFLO) superconductor [5–10], in a rotating superfluid [11, 12], in a moving polariton condensate [13] or in a sliding charge-density wave [14]. The one-dimensional Su-Schrieffer-Heeger (SSH) Hamiltonian with long-range hopping is a more recent example of a two-band system with modulated order parameter [15].

For a given microscopic model of interacting electrons, the superconducting order parameter is usually determined by the self-consistent mean-field (BCS) approach [16, 17], while the fluctuations out of the superconducting condensate of Cooper pairs are described by the BdG Hamiltonian. In this article we will focus on the quasiparticles and assume that the order parameter  $\Delta$  is obtained from the BCS approach. The BdG Hamiltonian can be expanded in terms of Pauli matrices as  $H_{\text{BdG}} = \vec{h}_{\text{BdG}} \cdot \vec{\sigma}$ , which belongs to a larger class of  $SU(2)$  Hamiltonians. In general, the  $SU(2)$  Hamiltonian of the form  $\vec{h} \cdot \vec{\sigma}$  has been used as a prototype for topological states in condensed matter to describe a number of fascinating properties in special materials, ranging from 2D graphene-like materials (e.g., the Haldane model) to 3D Weyl semimetals [18–26]. An interpretation of this Hamiltonian is that of a spin  $\vec{\sigma}$  is coupled to a (operator valued) pseudomagnetic field  $\vec{h}$ . Many of the specific properties of this type of Hamiltonian and its eigenfunctions originate in the robust winding number of the spinor states. A deeper understanding of the connection between the  $SU(2)$  Hamiltonian and the winding number of the spinor reveals robust physical properties of systems that are governed by such a Hamiltonian. In particular, we will study in this article how the phase of the superconducting order parameter affects the winding number and how this can be described by a Bloch vector and a related topological invariant, which is an observable

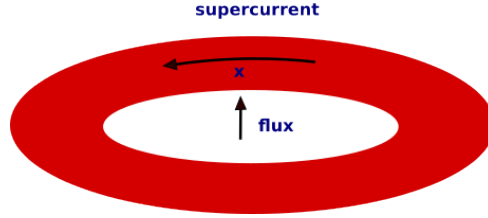


FIG. 1. A macroscopic vortex on a superconducting ring with radius  $R$ : the supercurrent induces a periodic order parameter  $\Delta(x) = |\Delta| \exp(ixn/R)$ , where the integers  $n = 0, \pm 1, \dots$  are enforced by the periodic boundary conditions in  $x$  direction. The specific value of  $n$  depends on the strength of the supercurrent, where an increasing supercurrent yields an increasing quantized winding number for the quasiparticle states.

quantity. In the discussion we distinguish between bulk and edge modes.

The winding number is often associated with a robust behavior due to its connection with topological invariants, for instance, in chiral quantum systems. Therefore, a weak perturbation might be insufficient for a change but we must rely on a strong and macroscopic intervention [27], usually caused by a symmetry change. What determines the winding number in a given system and how can we change it? And is it possible to control it by an external and macroscopic method? To answer these questions, we consider a ring made of a superconducting material, as schematically presented in Fig. 1), and apply a phase modulated order parameter. This can be understood as a macroscopic vortex in the superconducting state [28–30]. This is connected with the boundary conditions of the system, leading to a quantization of the order parameter phase. We will discuss how the latter affects the quasiparticle properties, which are subject to the BdG Hamiltonian.

The article is organized as follows. In Sect. II the BdG Hamiltonian, its energy dispersion and its eigenspinors are defined and discussed. Then the Bloch vector, a topological invariant for the winding number on the Bloch sphere and the order-parameter phase transformation are discussed in Sect. II A. After this general part, in Sect. III we turn to two specific realizations of the BdG Hamiltonian: in Sect. III A we study it in the continuum and in Sect. III B for the tight-binding realization on the square lattice. Edge modes and their relations with the bulk modes are discussed in Sect. IV. Finally, in Sect. V the results of the BdG Hamiltonian are summarized and compared with the  $\pi$ -flux Hamiltonian.

## II. MODEL

A large class of two-dimensional systems is described by the  $SU(2)$  Hamiltonian  $\vec{h} \cdot \vec{\sigma}$  with the Pauli vector  $\vec{\sigma} = (\sigma_1, \sigma_2, \sigma_3)^T$  and with the three-dimensional vector [18–25]

$$\vec{h} = (\Delta', \Delta'', D)^T, \quad (1)$$

where each vector component can be a self-adjoint differential operator. For the following study, however, we focus on the case where only  $D$  is a differential or difference operator on a two-dimensional space with coordinates  $(x, y)$ , while  $\Delta', \Delta''$  are the real and imaginary parts of a periodic function  $\Delta(x)$  in space.  $\Delta = \Delta' + i\Delta''$  can be considered as a complex order parameter, as it appears in the BdG Hamiltonian. Specific examples are discussed in Sect. III. We assume that there is a pair of complex numbers  $\gamma_j$  ( $j = 1, 2$ ) with  $De^{\gamma_j x} = d(\gamma_j)e^{\gamma_j x}$ . In other words,  $e^{\gamma_j x}$  is eigenfunction of  $D$  with a real eigenvalue  $d(\gamma_j)$ . With  $\Delta(x) = |\Delta|e^{ix/L}$  and a uniform  $|\Delta|$  we introduce the spinor

$$\Psi(x) = \begin{pmatrix} a_1 e^{\gamma_1 x} \\ a_2 e^{\gamma_2 x} \end{pmatrix} \quad (2)$$

to formulate the energy eigenvalue problem  $\vec{h} \cdot \vec{\sigma} \Psi_x = E \Psi_x$  in  $2 \times 2$  matrix notation as

$$\begin{pmatrix} d(\gamma_1)a_1 e^{\gamma_1 x} + |\Delta|a_2 e^{(\gamma_2 - i/L)x} \\ |\Delta|a_1 e^{(\gamma_1 + i/L)x} - d(\gamma_2)a_2 e^{\gamma_2 x} \end{pmatrix} = E \begin{pmatrix} a_1 e^{\gamma_1 x} \\ a_2 e^{\gamma_2 x} \end{pmatrix} \quad (3)$$

with a real eigenvalue  $E$ . Since the order parameter  $\Delta(x)$  is periodic with the period  $2\pi L$ , it reduces the translation-invariance but still has periodic eigenfunctions. The equation is satisfied for all  $x$  when  $\gamma_2 = \gamma_1 + i/L$  and

$$\frac{a_2}{a_1} = \frac{E - d(\gamma_1)}{|\Delta|}, \quad \frac{a_1}{a_2} = \frac{E + d(\gamma_2)}{|\Delta|}. \quad (4)$$

After dropping the index of  $\gamma_1$  (i.e.,  $\gamma \equiv \gamma_1$ ) the operator-valued  $\vec{h}$  in Eq. (1) becomes a number-valued vector through

$$H = d_+(\gamma)\sigma_0 + \vec{h} \cdot \vec{\sigma} \quad \text{with} \quad \vec{h} = (\Delta', \Delta'', d_-(\gamma))^T \quad (5)$$

and  $d_{\pm} = [d(\gamma) \pm d(\gamma + i/L)]/2$  and the  $2 \times 2$  unit matrix  $\sigma_0$ . Eq. (4) implies the quadratic equation in  $E$

$$[E - d(\gamma)][E + d(\gamma + i/L)] = |\Delta|^2, \quad (6)$$

which gives the dispersions

$$E_{\pm}(\gamma) = \frac{d(\gamma) - d(\gamma + i/L)}{2} \pm \frac{1}{2} \sqrt{[d(\gamma) + d(\gamma + i/L)]^2 + 4|\Delta|^2} \quad (7)$$

as the solutions. It is crucial that the values of  $\gamma$  are restricted such that  $E_{\pm}(\gamma)$  is real, since the Hamiltonian is Hermitian. Moreover, for a uniform phase, i.e. for  $L \rightarrow \infty$ , this dispersion reduces to  $E_{\pm} = \pm \sqrt{d(\gamma)^2 + |\Delta|^2}$ . The corresponding eigenfunctions are obtained from the spinor in Eq. (2) as

$$\Psi_E(x) = a_1 \left( \frac{e^{-ix/2L}}{|E-d(\gamma)|} e^{ix/2L+i\alpha} \right) e^{(\gamma+i/2L)x}, \quad (8)$$

where  $\alpha$  is the phase of  $a_2/a_1$ . It is important to note that a solution with  $\text{Re}(\gamma) \neq 0$  decays or grows exponentially with  $x$ . Therefore, such solutions can only exist on sample edges. In other words, if the system has no edges (e.g. a torus) only solutions with imaginary  $\gamma$  are allowed.

### A. Bloch vector and winding number

Next we analyze the winding number of the spinor. First, we note that the spinor in Eq. (8) without the exponential factor is parametrized by the coordinate  $x$  and it is invariant under  $x \rightarrow x + 4n\pi L$  for an integer  $n$ . The winding number is observable and usually related to the Berry phase, where the latter can be calculated from the Berry connection [31, 32]. Alternatively, the spinor can also be associated with the three-dimensional Bloch vector

$$\vec{s}(x) = \frac{\Psi(x) \cdot \vec{\sigma} \Psi(x)}{\Psi(x) \cdot \Psi(x)}, \quad (9)$$

which is the expectation value of the Pauli vector  $\vec{\sigma}$ . In Maxwell theory this vector is known as the Stokes vector for the characterization of the electromagnetic field and provides the Pancharatnam phase [33–35]. It is directly linked to the Berry curvature of the electromagnetic field [36]. In the present case the winding of the spinor can be associated with the three-dimensional Bloch vector of Eq. (9). Its components characterize the algebraic relations between the two spinor components of the solution  $\Psi_E(x)$  of Eq. (8):

$$s_1 = \frac{2b}{1+b^2} \cos(x/L + \alpha), \quad s_2 = \frac{2b}{1+b^2} \sin(x/L + \alpha), \quad s_3 = \frac{1-b^2}{1+b^2}, \quad (10)$$

where  $b = |a_2/a_1| = |E - d(\gamma)|/|\Delta|$ . The Bloch vector is invariant under  $x \rightarrow x + 2n\pi L$  for an integer  $n$ , which is half of the periodicity of the spinor. A closed trajectory along the  $x$ -direction on a torus or ring of length  $l$  maps onto the Bloch sphere as a trajectory with constant latitude that is determined by  $s_3$  and with the winding number  $w = l/2\pi L$ . Thus, the winding number depends only on the order parameter phase, while the radius of the trajectory  $2b/(1+b^2)$  depends on  $\gamma$  and  $E$ . Boundary conditions restrict

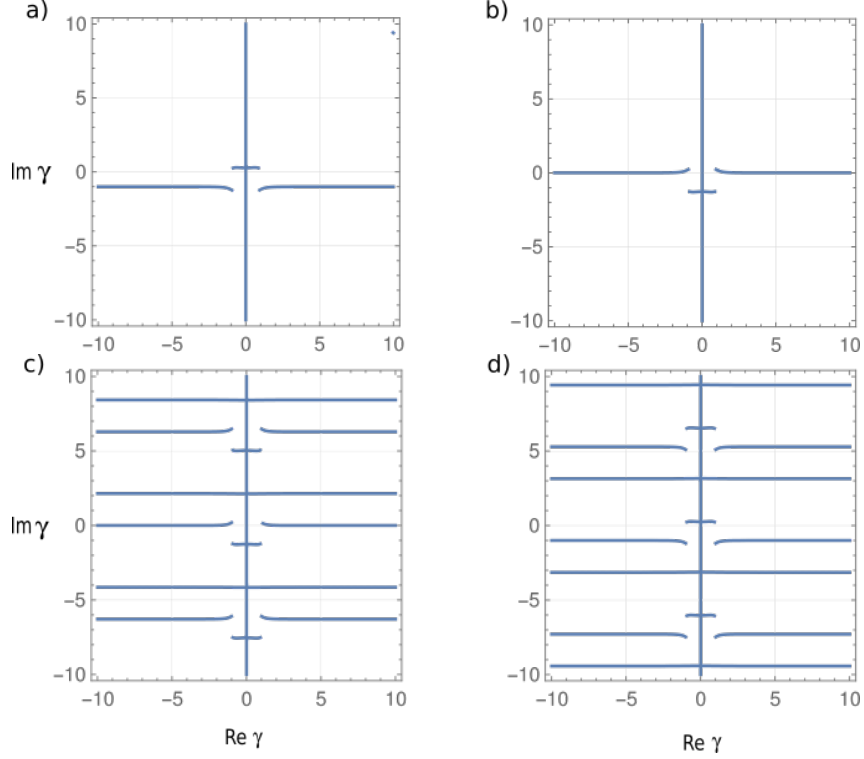


FIG. 2. Real-E spectrum: The blue curves present values of the complex wave number  $\gamma$ , where  $E_{\pm}(\gamma)$  is real. In this example the model parameters are  $|\Delta| = L = 1$ . Continuum model: a)  $E_+(\gamma)$  and b)  $E_-(\gamma)$ . Tight-binding model: c)  $E_+(\gamma)$  and d)  $E_-(\gamma)$ . The vertical lines with  $\text{Re}\gamma = 0$  represent the plane-wave solutions, while the other curves represent exponential solutions. The actual value of  $E_{\pm}(\gamma)$  is not indicated here but can be calculated separately: In Fig. 3b) some real energies for  $E_+(\gamma)$  of the tight-binding Hamiltonian in c) are presented. Examples for  $E_{\pm}(\gamma)$  along the vertical line in b) and c) are plotted in Fig. 4.

the parameter  $L$ . Here we assume periodic boundary conditions, such that we get  $L = l/2\pi n$  with integer  $n$ , which implies  $w = n$ . This means that we can determine the integer winding number by choosing the phase of the order parameter  $x/L$ . For  $E = d(\gamma)$ , where  $b = 0$ , the Bloch vector is on the north pole of the Bloch sphere, while for  $b = 1$  it is on the equator, and moves to the southern hemisphere for  $b > 1$ .

Only the first two components of  $\vec{s}$  depend on the phase of  $z$ , the third component is real because it is the expectation value of the diagonal matrix  $\sigma_3$ . Since the winding number is determined by the phase, for a fixed  $|z|$  we can calculate it using the  $s_1 - s_2$  - projected trajectory. In general, we can express the winding number of the Bloch vector with respect to the north-south axis of the Bloch sphere as the integral

$$w = \frac{1}{2\pi} \int_0^{2\pi} \vec{e}_3 \cdot \left[ \vec{s} \times \frac{d\vec{s}}{d\alpha} \right] \frac{1}{s_1^2 + s_2^2} d\alpha = \frac{\epsilon_{3jk}}{2\pi} \int_0^{2\pi} \frac{s_j}{s_1^2 + s_2^2} \frac{ds_k}{d\alpha} d\alpha. \quad (11)$$

The unit vector  $\vec{e}_3$  defines the north-south axis of the Bloch sphere and  $\epsilon_{ijk}$  is the Levi-Civita tensor. As explained in App. A, this integral links the Bloch vector directly with the winding number  $w$ .

Finally, we note that the unitary transformation

$$\vec{h} \cdot \vec{\sigma} \rightarrow \begin{pmatrix} e^{i\varphi/2} & 0 \\ 0 & e^{-i\varphi/2} \end{pmatrix} \begin{pmatrix} D & |\Delta| \\ |\Delta| & -D \end{pmatrix} \begin{pmatrix} e^{-i\varphi/2} & 0 \\ 0 & e^{i\varphi/2} \end{pmatrix} = \begin{pmatrix} \tilde{D} & |\Delta|e^{i\varphi} \\ |\Delta|e^{-i\varphi} & -\tilde{D}^* \end{pmatrix}, \quad \tilde{D} = e^{i\varphi/2} D e^{-i\varphi/2} \quad (12)$$

creates the phase factors for the order parameter by a simultaneous transformation of the operator  $D$ . In other words, this transforms the real order parameter  $|\Delta|$  of the Hamiltonian to a complex order parameter  $\Delta$ , which is accompanied by the creation of the self-adjoint operator  $\tilde{D}$ , whose eigenvalues

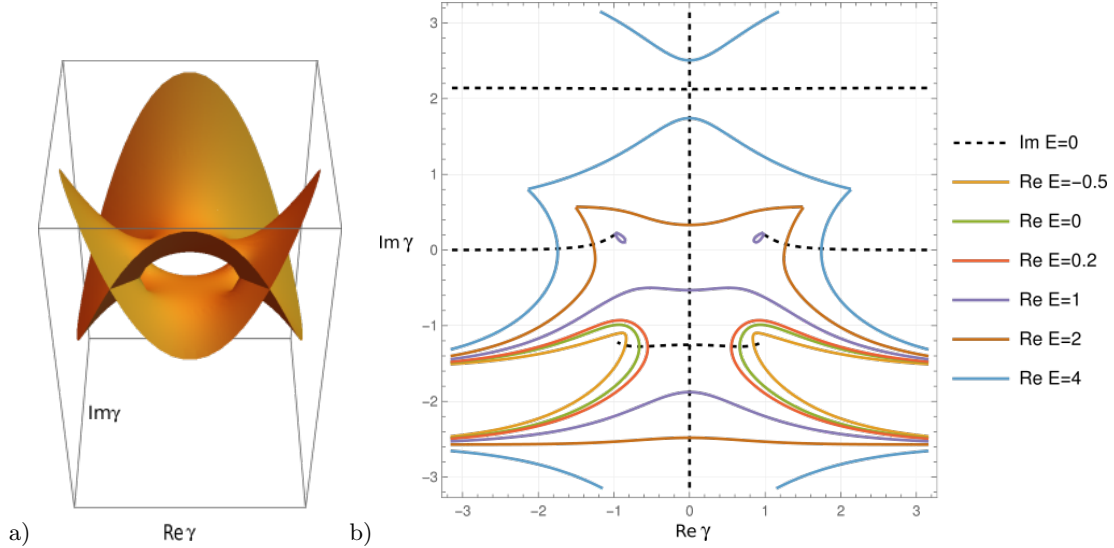


FIG. 3. a) Riemann surface of the real part  $\text{Re}E$  of the complex energy  $E$  of the continuous BdG Hamiltonian in Eq. (17) with  $|\Delta| = L = 1$ . It is symmetric with respect to  $\text{Re}\gamma$ . b) Contour plot of the complex spectrum: The dashed contours indicate  $\text{Im}E = 0$ , the other contours represent constant  $\text{Re}E$ . The curve crossings represent real eigenvalues of the tight-binding BdG Hamiltonian, whose values are color encoded.

are the same as those of  $D$ . Thus, the eigenfunctions and the structure of the spinor as well as the Bloch vector and its winding number are transformed. In Sect. V we will discuss how such a unitary transformation is related to the Bloch vector.

Many physical quantities depend only on the spectral properties of the Hamiltonian. For instance, trace expressions such as the thermodynamic quantities or the density of states. This is also the case for expressions represented by an inner product. These quantities are invariant under unitary transformations. Correlation functions, on the other hand, may not be invariant under general unitary transformations, such as the relation of the spinor components in Eqs. (2) or (8), whose real and imaginary parts are observable.

### III. BOGOLIUBOV DE GENNES HAMILTONIANS

In the following we will consider two examples for the operator  $D$ , namely the BdG Hamiltonian in a continuous space and its tight-binding version on a square lattice. The BdG Hamiltonian with different symmetries have been intensively studied for translation-invariant systems [37–39]. We will rely here on its simplest form but break the translational invariance by a periodic order parameter  $\Delta(x)$ , as introduced in the previous section. The existence of a spatially modulated order parameter with a characteristic wave vector  $\mathbf{q}$  is known from the Fulde-Ferrell-Larkin-Ovchinnikov (FFLO) phase of a superconductor in a magnetic field [5, 6].  $\mathbf{q}$  is determined by the linearized gap equation and depends on the external magnetic field, the temperature and the Fermi surface [10]. A simpler realization is the superconducting ring of Fig. 1, where the order-parameter oscillations are induced by a supercurrent.

#### A. Continuous BdG Hamiltonian

We choose the  $SU(2)$  Hamiltonian  $\vec{h}_{BdG} \cdot \vec{\sigma}$  with  $D = -\partial_x^2 - \partial_y^2$  acting on a finite continuous space:

$$\vec{h}_{BdG} = (\Delta', \Delta'', -\partial_x^2 - \partial_y^2). \quad (13)$$

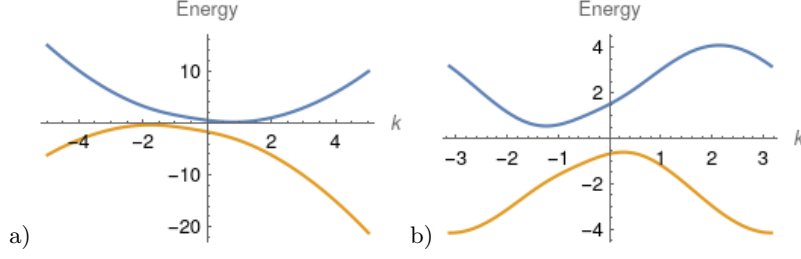


FIG. 4. Energy dispersion  $E_{\pm}(k)$  of the plane-wave solution for a) the continuous BdG Hamiltonian and b) for the tight-binding BdG Hamiltonian with  $|\Delta| = L = 1$ . These dispersions correspond to the vertical lines in Fig. 2.

When we assume that  $\Delta$  is uniform in the  $y$  direction, we can apply the Fourier transformation  $-\partial_y^2 \rightarrow k_y^2$ . The corresponding eigenvalue problem of the quasiparticles with energy  $E$  reads as the BdG equation

$$\begin{pmatrix} -\partial_x^2 + k_y^2 & |\Delta|e^{ix/L} \\ |\Delta|e^{-ix/L} & \partial_x^2 - k_y^2 \end{pmatrix} \begin{pmatrix} \psi_1 \\ \psi_2 \end{pmatrix} = E \begin{pmatrix} \psi_1 \\ \psi_2 \end{pmatrix}, \quad (14)$$

whose solutions describe the wavefunctions along a torus or a cylinder in the  $x$  direction, respectively. For the BdG Hamiltonian a spatial variation of the phase induces a supercurrent  $\mathbf{j}_s$  and vice versa, based on the Ginzburg-Landau supercurrent-phase relation [17]

$$\mathbf{j}_s = \frac{\hbar e^*}{m^*} |\Delta|^2 (\nabla\varphi - \frac{e^*}{\hbar c} \mathbf{A}) \quad (15)$$

in the presence of a vector potential  $\mathbf{A}$ .  $e^*$  and  $m^*$  are the charge and the mass of the Cooper pairs. This relation provides the unitary transformation in Eq. (12) by an appropriate choice of the supercurrent and the vector potential. In particular, the special choice  $\varphi = x/L$  creates the phase of Eq. (14). The supercurrent is only indirectly connected to the winding number through the gradient of the phase  $\varphi$ , but does not depend on itself. Thus, this current does not provide information of the winding number. On the other hand, we note that the quasiparticle currents depend on the winding number. They were studied explicitly, for instance, in Ref. [40].

Neglecting the vector potential in Eq. (15), the phase gradient  $\nabla\varphi$  is proportional to the supercurrent. This suggests that we obtain  $\varphi = x/L$  when we create a constant supercurrent in  $x$ -direction with the help of an external field. An experimental realization would be a superconducting ring, as illustrated in Fig. 1, which is reminiscent of a macroscopic vortex. The resulting phase jump is not a problem as long as the order parameter is continuous, since the phase is not observable due to the  $U(1)$  symmetry of the superconductor.

From Sect. II we get for this special case the  $\gamma \rightarrow -\gamma$  symmetric eigenvalues  $d(\gamma) = -\gamma^2 + k_y^2$  and Eq. (6) for the energy eigenvalues becomes

$$[E + \gamma^2 - k_y^2][E - (\gamma + i/L)^2 + k_y^2] = |\Delta|^2. \quad (16)$$

Moreover, considering a constant solution in  $y$  direction (i.e.,  $k_y = 0$ ), we obtain as the solution of the quadratic equation  $(E + \gamma^2)[E - (\gamma + i/L)^2] = |\Delta|^2$  for  $E$  the dispersion

$$E_{\pm}(\gamma) = \frac{i\gamma}{L} - \frac{1}{2L^2} \pm \frac{1}{2} \sqrt{[\gamma^2 + (\gamma + i/L)^2]^2 + 4|\Delta|^2}. \quad (17)$$

This is not symmetric under  $\gamma \rightarrow -\gamma$  but its real part is symmetric with respect to  $\text{Re}\gamma \rightarrow -\text{Re}\gamma$  (cf. Fig. 3). With  $\gamma = \kappa + ik$ , where  $k$  and  $\kappa$  are real, we can distinguish plane-wave solutions for  $\kappa = 0$  and exponential solutions for  $\kappa \neq 0$ . Exponential means here that the absolute value of the solution either decreases or increases exponentially with  $x$ . Employing the plane-wave solution  $\gamma = ik$  we obtain  $(E - k^2)[E + (k + 1/L)^2] = |\Delta|^2$ . This gives for the dispersion in Eq. (17)

$$E_{\pm}(ik) = -\frac{k}{L} - \frac{1}{2L^2} \pm \frac{1}{2} \sqrt{[k^2 + (k + 1/L)^2]^2 + 4|\Delta|^2}, \quad (18)$$

which is real for any  $k$  with  $-\infty < k < \infty$ . This dispersion is plotted in Fig. 4a) for  $|\Delta| = L = 1$ . Expansion for small  $k$  yields a gap and a linear  $k$  term, while the asymptotic behavior for large  $k$  is parabolic:

$$E_{\pm} \sim \pm k^2. \quad (19)$$

For the zero mode  $E = 0$  and  $k_y = 0$  we get directly from Eq. (16) the quartic equation  $\gamma^2(\gamma + i/L)^2 = -|\Delta|^2$  that reduces to the two quadratic equations  $\gamma(\gamma + i/L) = \pm i|\Delta|$  with the four solutions

$$\gamma = -\frac{i}{2L} \pm i\sqrt{i|\Delta| + 1/4L^2} \quad \text{and} \quad \gamma' = -\frac{i}{2L} \pm i\sqrt{-i|\Delta| + 1/4L^2}. \quad (20)$$

These solutions are exponential for  $|\Delta| > 0$ , since we have a gap for the plane-wave solution. There are other exponential solutions for real  $E \neq 0$ , as indicated by the horizontal blue curves on the complex  $\gamma$  plane in Figs. 2 a), b). The corresponding values of  $E$  along these curves are not indicated in these two-dimensional plots, but are plotted separately in Fig. 3b) for some characteristic values of  $\gamma$ .

The unitary transformation of Eq. (12) implies in this case

$$-\partial_x^2 \rightarrow (i\partial_x + 1/2L)^2, \quad (21)$$

where  $1/2L$  represents a gauge field. This reflects the relation in Eq. (15) in terms of the quasiparticle Hamiltonian, in which an additional gauge field changes the gradient of the order-parameter phase.

Finally, for the plane-wave solutions we have  $b = |E - k^2|/|\Delta|$  in Eq. (10). The winding number for the ring-like geometry in Fig. 1 is determined by the integral in Eq. (11): The integration is parametrized in this case with  $\alpha = x/R$  along the ring's circumference  $2\pi R$ , where  $R$  is the radius of the ring. Periodic boundary conditions on the ring require  $R/L = n$  with  $n = 0, \pm 1, \dots$ , and yield the winding number  $w = n$ . This means that the winding numbers in the upper and in the lower band are the same.

## B. Tight-binding BdG Hamiltonian on a square lattice

In general, the spectral properties of a system in the continuum and on a lattice are quite different. We will study next whether this is also the case for the Bloch vector of the BdG Hamiltonian. To this end we consider the case in which  $D$  is a difference operator with  $D\psi_x = \psi_{x+1} + \psi_{x-1} - 2\psi_x$  that acts on a discrete lattice with unit lattice spacing. Here we have only considered the  $x$  direction, the  $y$  direction is analogue. Its eigenvalue condition reads in this case

$$De^{\gamma_j x} = e^{\gamma_j(x+1)} + e^{\gamma_j(x-1)} - 2e^{\gamma_j x} = 2(\cosh \gamma_j - 1)e^{\gamma_j x}, \quad (22)$$

such that  $d(\gamma) = 2(\cosh \gamma - 1)$  is symmetric with respect to  $\gamma \rightarrow -\gamma$  and gives with Eq. (7) the dispersion

$$E_{\pm}(\gamma) = \cosh(\gamma) - \cosh(\gamma + i/L) \pm \sqrt{[\cosh(\gamma) + \cosh(\gamma + i/L) - 2]^2 + |\Delta|^2}, \quad (23)$$

which is complex for general  $\gamma$  and not symmetric. For  $\gamma = ik$  the plane-wave dispersion follows as

$$E_{\pm}(ik) = \cos k - \cos(k + 1/L) \pm \sqrt{[\cos(k) + \cos(k + 1/L) - 2]^2 + |\Delta|^2}, \quad (24)$$

which is real again for any  $k$  with  $-\pi \leq k < \pi$ . The dispersion  $E_{\pm}(ik)$  is visualized in Fig. 4b). There are also exponential solutions with a real dispersion. They have nonzero  $\text{Re}\gamma$  values and are indicated as horizontal curves in Figs. 2 c) and d).

Inserting the eigenvalues  $d(\gamma)$  into the spinor of Eq. (8) and into the Bloch vector of Eq. (10) enables us to calculate the winding number for the tight-binding BdG Hamiltonian. For plane-wave solutions  $b = |a_2/a_1| = |E - d(\gamma)|/|\Delta| = |E - 2(\cos k - 1)|/|\Delta|$ . Thus, the Bloch vector is affected by the introduction of a lattice. However, since  $b$  does not depend on  $x$ , it drops out of the integrand in Eq. (11), and we get the same winding number as in the continuum case. Finally, the unitary transformation of Eq. (12) reads in this case

$$\tilde{D}\psi_x = e^{-i/2L}\psi_{x+1} + e^{i/2L}\psi_{x-1} - 2\psi_x, \quad (25)$$

where  $i/2L$  represents a Peierls phase on the hopping elements in  $x$  direction, in analogy with the gauge transformation of the continuous BdG Hamiltonian in Eq. (21).

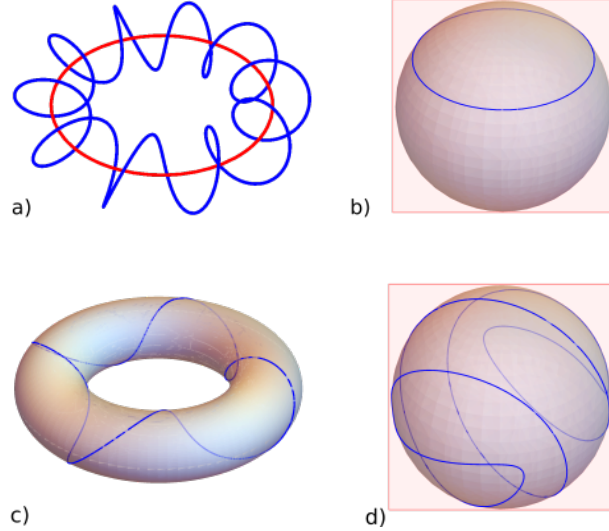


FIG. 5. Top row is for the BdG Hamiltonian: a) A superconducting order parameter  $(\Delta', \Delta'') = (\cos(10x), \sin(10x))$  with  $0 \leq x < 2\pi$  (blue) along a superconducting ring (red) implies b) a map on the Bloch sphere. The winding number of this trajectory is  $w = 10$ ; i.e., the trajectory winds 10 times around the Bloch sphere. The latitude on the Bloch sphere depends on the parameter  $b$ , which is  $b = 1/2$  in this example. Bottom row is for the  $\pi$ -flux Hamiltonian: c) a closed helical trajectory on a torus with  $n_x = 4$ ,  $n_y = 1$  windings and d) its map on the Bloch sphere. The winding number of this trajectory with respect to the north-south axis of the Bloch sphere is  $w = 0$ .

#### IV. EXPONENTIAL SOLUTIONS

To find the exponential eigenfunctions, we can either solve Eq. (6) directly or employ the analytic bulk-edge connection [40, 41]. The eigenvalues  $d(\gamma) = -\gamma^2$  of the continuous BdG Hamiltonian and  $d(\gamma) = 2(\cosh \gamma - 1)$  of the tight-binding BdG Hamiltonian are both real for real as well as purely imaginary  $\gamma$ , while the dispersions in Eq. (17) and in Eq. (23) are real only for purely imaginary  $\gamma$ . This suggests that the analytic continuation starts from a plane-wave (bulk) solution. Then the analytic continuation  $ik \rightarrow \gamma$  of the real wave number  $k$  into the complex plane is applied. In general, this leads to a complex energy, which violates the eigenvalue equation for real energies. Therefore, the additional condition of a real  $E_{\pm}(\gamma)$  must be enforced. The results of the analytic bulk-edge connection are visualized in Figs. 2 a) – d): For the continuous BdG Hamiltonian we obtain the real-E curves in Figs. 2 a), b), while the tight-binding BdG Hamiltonian gives Figs. 2 c), d). In both cases the vertical lines at  $\text{Re}\gamma = 0$  represent the plane-wave solutions, while the other curves represent exponential solutions. The periodic behavior of the tight-binding spectrum in Eq. (24) for imaginary  $\gamma$  is reflected by the repeated real-E curves in Figs. 2c), d). Apart from this feature, the real-E spectrum is similar for both Hamiltonians and their real-E curves are symmetric with respect to  $\text{Re}\gamma \rightarrow -\text{Re}\gamma$ .

The Bloch vector in Eq. (10) is valid for plane-wave as well as for exponential solutions of Eq. (14), an exponential solution might have a phase shift  $\alpha \neq 0$  and a different  $b$  though. The winding number is directly linked to the phase of the order parameter  $x/L$ . In general, we might consider non-periodic boundary conditions, for instance, in a superconducting ring with a Josephson barrier. This indicates that the winding number of the bulk modes differ from those of the edge modes simply due to different boundary conditions. The latter depend on the specific set-up of the physical system. It is beyond the scope of the present work to elaborate on this experiment-specific issue. In any case, though, the boundary conditions must also lead to a self-adjoint Hamiltonian, which requires that the energy eigenstates for different eigenvalues are orthogonal.

## V. DISCUSSION AND SUMMARY

The mapping  $\vec{h}\cdot\vec{\sigma} \rightarrow \Psi \rightarrow \vec{s}$  of Sect. II, where  $\vec{h}\cdot\vec{\sigma}$  is the Hamiltonian,  $\Psi$  is an eigenspinor of  $\vec{h}\cdot\vec{\sigma}$  and  $\vec{s}$  is the three-dimensional Bloch vector, provides a triple of relevant quantities to characterize an  $SU(2)$ -based quantum system. The Bloch vector  $\vec{s}$  is an observable that visualizes the winding number of the quantum state. To study the effect of the order-parameter phase on the quasiparticles of a superconductor, we have introduced the periodic order parameter  $\Delta = |\Delta|e^{ix/L}$  with the parameter  $L$ , which induces the spatial winding number  $w$  of the Bloch vector.  $L$  depends on the boundary conditions and can be controlled in the case of the BdG Hamiltonian through the supercurrent as well as through the vector potential of an external electromagnetic field. The appearance of a periodic order-parameter phase can be linked with the picture of a macroscopic vortex. According to our discussion in Sect. III, the order parameter phase determines the winding number in the case of periodic boundary conditions. In Figs. 5a),b) an example with the order-parameter phase  $\varphi = 10x/2\pi$  and its corresponding trajectory on the Bloch sphere are depicted.

An important question regarding the observation of the winding number by using the Bloch vector is whether a closed Bloch-vector trajectory is always accompanied by closed spinor trajectory? The answer is no because this depends on the definition of the spinor. Our specific spinor definition in Eq. (8) indicates that the winding numbers do not agree: The spinor of Eq. (8) has the periodicity  $4n\pi L$  but the Bloch vector in Eq. (10) is periodic in  $x$  with period  $2n\pi L$ .

Winding numbers also appear without a periodic order parameter, for instance, in chiral systems. We briefly mention here the  $\pi$ -flux Hamiltonian [26] with

$$\vec{h} = (\sin k_x, \sin k_y, m \cos k_x \cos k_y)^T \quad (26)$$

and  $(k_x, k_y)$  on a torus. It describes a particle hopping on a square lattice with flux  $\pi$  per plaquette. We consider a closed helical trajectory on the torus that winds  $n_x$  times around the small circle and  $n_y$  around the large circle. An example with  $n_x = 4$  and  $n_y = 1$  is visualized in Fig. 5c). This trajectory is mapped onto the Bloch sphere, as demonstrated in Fig. 5d), which results in a twisted loop whose winding number is  $w = 0$  according to Eq. (11). This is also the case for other values of  $n_x \geq 1$ . In contrast to the rotation of the order-parameter phase in the BdG Hamiltonian, an increasing  $n_x$  on the torus does not result in an increasing  $w$  for the  $\pi$ -flux Hamiltonian. On the other hand, a non-helical loop on the torus, e.g., one with  $n_x = n_y = 0$ , has a winding number  $w = 1$  or  $w = -1$ , depending on the position of the loop center on the torus. Thus, the winding number in the  $\pi$ -flux Hamiltonian is robust with  $w = 0, \pm 1$ , only depending on the trajectory on the torus.

The effect of a winding spinor can be described by employing the unitary transformation in Eq. (12). This transformation transfers the phase from the eigenspinor to the Pauli vector (cf. App. B):

$$s_1 \rightarrow \bar{s} \cos \varphi, \quad s_2 \rightarrow \bar{s} \sin \varphi \quad (27)$$

with the same real coefficient  $\bar{s}$ . Then Eq. (11) implies for the winding number

$$w = \frac{\varphi(2\pi) - \varphi(0)}{2\pi}, \quad (28)$$

where the parametrization  $\varphi(\alpha)$  of the phase with  $0 \leq \alpha < 2\pi$  has been used. This phase depends on the specific model we consider and the special closed trajectory. For the BdG Hamiltonian on a superconducting ring it depends on the superconducting order parameter, while for the  $\pi$ -flux Hamiltonian it is determined by the trajectory on the torus of the underlying physical space. An example is a small loop for the  $\pi$ -flux Hamiltonian, which gives  $\varphi(\alpha) = \alpha$  for a loop centered at  $k_x = k_y = 0$  or  $\varphi(\alpha) = -\alpha$  for a loop centered at  $k_x = 0, k_y = \pi$ , leading to  $w = \pm 1$  according to Eq. (28). This case is related to the corresponding Chern number, which effectively calculates a simple closed loop without winding around the torus through the Berry curvature [26].

Focusing on the BdG Hamiltonian, a giant vortex can be created on a superconducting disk [28, 29] or on a superconducting ring [30], which provides the modulated order-parameter phase. In such a system it should be possible to study the properties of the quasiparticles as a function of the vorticity. As an observable, the Bloch vector is experimentally accessible through linear response with respect to the order parameter. In particular, we get from a change of the energy eigenvalues the first two components of the Bloch vector as  $s_1 = \partial_{\Delta'} E$  and  $s_2 = \partial_{\Delta''} E$  [42]. They are relevant for the winding

number, and we can insert them directly into Eq. (11). The single-ring geometry can be extended to a network of superconducting links as a host of several vortices. This system represents a more complex order parameter for topologically protected quasiparticles, which could be useful for robust quantum-technological applications.

Finally, it should be emphasized that the Hamiltonians discussed in this work are Hermitian. An extension by including non-Hermitian terms, as used in the concept of “non-Bloch BdG Hamiltonians” [43, 44], might be interesting but should be left for future projects. In particular, to compare the role of edge modes in the Hermitian case with their role in the non-Hermitian case could offer new insights into the effect of the environment on the quantum system. Another extension of the present work could be based on other order parameters. For instance, we can consider piecewise linear phases on short intervals with alternating slopes  $\varphi = \pm x/L$ , where the phase is still continuous. The matching of the eigenfunctions at the sign-switching points creates additional exponential solutions, creating a special kind of localized wave function. Moreover, if the steps between sign switches are random, this mimics a random phase similar to those in disordered systems.

### Appendix A: Winding number as an invariant on the Bloch sphere

We consider a Bloch sphere whose north-south axis is parallel to the unit vector  $\vec{e}_3$  and the Pauli matrix  $\sigma_3$  is the  $2 \times 2$  diagonal matrix. The Bloch vector is parametrized as usual with the two angles  $\varphi, \theta$  as

$$\vec{s} = \begin{pmatrix} \cos \varphi \sin \theta \\ \sin \varphi \sin \theta \\ \cos \theta \end{pmatrix}. \quad (\text{A1})$$

Both angles depend on the parameter  $\alpha$  with the same values at  $\alpha = 0$  and  $\alpha = 2\pi$ . Then we define the winding around the 3-axis as the integral

$$w := \frac{1}{2\pi} \int_0^{2\pi} \vec{e}_3 \cdot \left[ \vec{s} \times \frac{d\vec{s}}{d\alpha} \right] \frac{1}{s_1^2 + s_2^2} d\alpha = \frac{\epsilon_{3jk}}{2\pi} \int_0^{2\pi} \frac{s_j}{s_1^2 + s_2^2} \frac{ds_k}{d\alpha} d\alpha. \quad (\text{A2})$$

Here  $\sqrt{s_1^2 + s_2^2}$  is the normalization of the vector  $(s_1, s_2)^T$ . This integral acts only on the  $s_1 - s_2$  projected Bloch vector, which is a consequence of the fact that the third vector component  $s_3$  is the reference axis for the winding of the spinor. Therefore,  $s_3$  does not contribute due to the Levi-Civita tensor  $\epsilon_{3jk}$ . Moreover, the differential with respect to  $\theta$  drops out due to

$$s_2 \frac{ds_1}{d\theta} = s_1 \frac{ds_2}{d\theta}. \quad (\text{A3})$$

Thus, we get from Eq. (A1)

$$w = \frac{1}{2\pi} \int_0^{2\pi} (\cos^2 \varphi + \sin^2 \varphi) \frac{d\varphi}{d\alpha} d\alpha = \frac{1}{2\pi} \int_0^{2\pi} \frac{d\varphi}{d\alpha} d\alpha = \frac{\varphi(2\pi) - \varphi(0)}{2\pi}. \quad (\text{A4})$$

This is the winding number. We note that  $\vec{s}(\alpha)$  can be a multi-valued function on the interval  $[0, 2\pi)$ . For instance, with  $\varphi = n\alpha$  we get for the integral  $w = n$ .

It should be noted that there is an ambiguity in the choice of  $\vec{e}_3$ . Instead of using the south pole as the reference point of the coordinate system, we could also choose the center of the Bloch sphere. Then the winding numbers differ by a sign change between the southern and the northern hemisphere.

### Appendix B: The $2 \times 2$ matrix structure

There is an intimate connection between spinors and winding numbers. As an instructive demonstration of this connection, we consider the  $2 \times 2$  Hamiltonian

$$H_0 = \begin{pmatrix} m & z \\ z^* & -m \end{pmatrix} = \vec{h}_0 \cdot \vec{\sigma} \quad (\text{B1})$$

with  $m$  real,  $z = z' - iz''$  and real  $z', z''$ . The vector  $\vec{\sigma} = (\sigma_1, \sigma_2, \sigma_3)$  comprises the Pauli matrices and  $\vec{h}_0 = (z', z'', m)$ . The corresponding eigenvalue problem with eigenvalue  $E = \pm\sqrt{m^2 + |z|^2}$  reads

$$\begin{pmatrix} m & z \\ z^* & -m \end{pmatrix} \begin{pmatrix} a_1 \\ a_2 \end{pmatrix} = E \begin{pmatrix} a_1 \\ a_2 \end{pmatrix},$$

which separates into two equations

$$\begin{cases} a_1 = \frac{z}{E-m} a_2 \\ a_2 = \frac{z^*}{E+m} a_1 \end{cases}.$$

A solution of these equations is the spinor

$$\Psi = a_1 \begin{pmatrix} 1 \\ z^*/(E+m) \end{pmatrix} = a_1 \begin{pmatrix} 1 \\ (E-m)/z \end{pmatrix}. \quad (\text{B2})$$

The related Bloch vector is of unit length and its components read

$$s_1 = \frac{2z'}{\mathcal{N}_0(E+m)}, \quad s_2 = \frac{2z''}{\mathcal{N}_0(E+m)}, \quad s_3 = \frac{1}{\mathcal{N}_0} \left[ 1 - \frac{|z|^2}{(E+m)^2} \right] \quad (\text{B3})$$

with the normalization  $\mathcal{N}_0 = 1 + |z|^2/(E+m)^2$ . This means that a closed trajectory of  $z$  on the complex plane or on some Riemann sheets maps onto a closed trajectory on the Bloch sphere.

The Hamiltonian matrix  $H_0$  in Eq. (B1) reads for  $z = |z|e^{i\varphi}$

$$U_0 \begin{pmatrix} m & |z| \\ |z| & -m \end{pmatrix} U_0^\dagger \quad \text{with} \quad U_0 = \begin{pmatrix} e^{i\varphi/2} & 0 \\ 0 & e^{-i\varphi/2} \end{pmatrix}. \quad (\text{B4})$$

Thus,  $U_0^\dagger H_0 U_0$  and its eigenspinors do not depend on the phase  $\varphi$ . Moreover, this unitary transformation implies a unitary transformation of the Pauli vector in the Bloch vector of Eq. (9):  $\vec{\sigma} \rightarrow U_0^\dagger \vec{\sigma} U_0$ . Since the eigenspinors of  $U_0^\dagger H_0 U_0$  are real and do not depend on the phase  $\varphi$ , we get for the Bloch vector

$$s'_1 = \frac{2\psi_1\psi_2}{\psi_1^2 + \psi_2^2} \cos \varphi, \quad s'_2 = \frac{2\psi_1\psi_2}{\psi_1^2 + \psi_2^2} \sin \varphi, \quad s'_3 = \frac{\psi_1^2 - \psi_2^2}{\psi_1^2 + \psi_2^2}. \quad (\text{B5})$$

- 
- [1] A.A. Abrikosov. *The magnetic properties of superconducting alloys*, Journal of Physics and Chemistry of Solids 2, 199 (1957).
  - [2] B. Josephson. *Possible new effects in superconductive tunnelling*, Physics Letters 1, 251 (1962).
  - [3] G. E. Blonder, M. Tinkham, and T. M. Klapwijk. *Transition from metallic to tunneling regimes in superconducting microconstrictions: Excess current, charge imbalance, and supercurrent conversion*, Phys. Rev. B, 25:4515–4532 (1982).
  - [4] A. Spuntarelli, P. Pieri, and G.C. Strinati. *Solution of the bogoliubov–de gennes equations at zero temperature throughout the bcs–bec crossover: Josephson and related effects*, Physics Reports, 488(4):111–167 (2010).
  - [5] P. Fulde and R. Ferrell. *Superconductivity in a Strong Spin-Exchange Field*, Phys. Rev. 135, A550 (1964).
  - [6] A.I. Larkin and Y.N. Ovchinnikov. *Nonuniform state of superconductors*, Zh. Eksp. Teor. Fiz. 47, 1136 (1964) [Sov. Phys. JETP 20, 762 (1965)].
  - [7] Z. Zheng, M. Gong, X. Zou, C. Zhang, and G. Guo. *Route to observable Fulde-Ferrell-Larkin-Ovchinnikov phases in three-dimensional spin-orbit-coupled degenerate Fermi gases*, Phys. Rev. A 87, 031602(R) (2013).
  - [8] L.-F. Guo, P. Li, and S. Yi. *Topological Fulde-Ferrell superfluids in triangular lattices*, Phys. Rev. A 95, 063610 (2017).
  - [9] X. Zhang and F. Liu. *Fulde-Ferrell-Larkin-Ovchinnikov pairing induced by a Weyl nodal line in an Ising superconductor with a high critical field*, Phys. Rev. B 105, 024505 (2022).
  - [10] H. Shimahara. *Transition from the vortex state to the Fulde-Ferrell-Larkin-Ovchinnikov state in quasi-two-dimensional superconductors*, Phys. Rev. B 80, 214512 (2009).
  - [11] L. Tisza. *Transport phenomena in helium II*, Nature 141, 913 (1938).
  - [12] L. Landau. *Theory of the superfluidity of helium II*, Phys. Rev. 60, 356 (1941).

- [13] I. Carusotto and C. Ciuti. *Quantum fluids of light*, Rev. Mod. Phys. 85, 299 (2013).
- [14] G. Grüner. *The dynamics of charge-density waves*, Rev. Mod. Phys. 60, 1129 (1988).
- [15] H. Liu, X. Huang, M. Yan, J. Lu, W. Deng, and Z. Liu, *Acoustic Topological Metamaterials of Large Winding Number*, Phys. Rev. Applied 19, 054028 (2023).
- [16] J. Bardeen, L.N. Cooper, and J.R. Schrieffer. *Microscopic Theory of Superconductivity* Phys. Rev. 106, 162 (1957).
- [17] M. Tinkham. *Introduction to Superconductivity*, Dover Publications (1996).
- [18] F.D.M. Haldane. *Model for a Quantum Hall Effect without Landau Levels: Condensed-Matter Realization of the "Parity Anomaly"*, Phys. Rev. Lett. 61, 2015 (1988).
- [19] V.M. Yakovenko. *Chern-Simons Terms and  $n$  Field in Haldane's Model for the Quantum Hall Effect without Landau Levels*, Phys. Rev. Lett. 65, 251 (1990).
- [20] Y. Hatsugai. *Chern number and edge states in the integer quantum Hall effect*, Phys. Rev. Lett. 71, 3697 (1993).
- [21] C. L. Kane and E.J. Mele.  *$Z_2$  topological order and the quantum spin hall effect*, Phys. Rev. Lett. 95, 146802 (2005).
- [22] C.L. Kane and E.J. Mele. *Quantum spin hall effect in graphene*, Phys. Rev. Lett. 95, 226801 (2005).
- [23] B.A. Bernevig and S.C. Zhang. *Quantum spin hall effect*, Phys. Rev. Lett. 96, 106802 (2006).
- [24] N.P. Armitage, E.J. Mele and A. Vishwanath. *Weyl and Dirac semimetals in three-dimensional solids*, Rev. Mod. Phys. 90, 015001 (2018).
- [25] A.A. Burkov. *Weyl metals*, Annual Review of Condensed Matter Physics Volume 9, (2018).
- [26] E. Fradkin. *Field Theories of Condensed Matter Physics*, Cambridge University Press (2013).
- [27] Y. Aharonov and D. Bohm. *Significance of Electromagnetic Potentials in the Quantum Theory*, Phys. Rev. 115, 485–491 (1959).
- [28] V. Bruyndoncx, J. G. Rodrigo, T. Puig, L. Van Look, and V.V. Moshchalkov. *Giant vortex state in perforated aluminum microsquares*, Phys. Rev 60, 4285 (1999).
- [29] A. Kanda, B.J. Baelus, F.M. Peeters, K. Kadowaki, and Y. Ootuka. *Experimental Evidence for Giant Vortex States in a Mesoscopic Superconducting Disk*, Phys. Rev. Lett. 93, 257002 (2004).
- [30] J.X. Liu, L.M. Shi and G.-Q. Zha. *Giant vortex state in a mesoscopic superconducting thin ring*, Physica C 588, 1353917 (2021).
- [31] M. Berry. *Quantal Phase Factors Accompanying Adiabatic Changes*, Proceedings of the Royal Society A 392, 45 (1984).
- [32] B. Simon. *Holonomy, the Quantum Adiabatic Theorem, and Berry's Phase*, Phys. Rev. Lett. 51, 2167 (1983).
- [33] S. Pancharatnam. *Generalized theory of interference, and its applications*, Proc. Ind. Acad. Sci. A 44, 247 (1956).
- [34] M.V. Berry. *The adiabatic phase and Pancharatnam's phase for polarized light*, J. Mod. Opt. 34, 1401 (1987).
- [35] Y.B. Band, I. Kuzmenko, and Y. Avishai. *Geometric phases in optics: Polarization of light propagating in helical optical fibers*, Phys. Rev. A 111, 033530 (2025).
- [36] K. Ziegler. *Circular edge states in photonic crystals with a Dirac node*, J. Opt. Soc. Am. B 35, 107-112 (2018).
- [37] A. Skurativska, T. Neupert, M.H. Fischer. *Atomic limit and inversion-symmetry indicators for topological superconductors*, Phys. Rev. Research 2, 013064 (2020).
- [38] S. Ono, H.C. Po, and H. Watanabe. *Refined symmetry indicators for topological superconductors in all space groups* Science Advances 6 (18) (2020).
- [39] M. Geier, P.W. Brouwer, and L. Trifunovic. *Symmetry-based indicators for topological Bogoliubov–de Gennes Hamiltonians*, Phys. Rev. B 101, 245128 (2020).
- [40] K. Ziegler and R.Ya. Kezerashvili. *Edge modes in chiral electron double layers*, Phys. Rev. B 111, L140507 (2025).
- [41] K. Ziegler. *Analytic bulk-edge connection in circular-symmetric models*, J. Phys. A: Math. Theor. 58 345301 (2025).
- [42] Q. Liu and K. Ziegler. *Relation between winding numbers and energy dispersions*, arXiv:2512.23685 (2025).
- [43] S. Yao and Z. Wang. *Edge States and Topological Invariants of Non-Hermitian Systems*, Phys. Rev. Lett. 121, 086803 (2018).
- [44] K. Yokomizo and S. Murakami. *Non-Bloch band theory in bosonic Bogoliubov–de Gennes systems*, Phys. Rev. B103,165123 (2021).